Thermophoresis of colloids by mesoscale simulations

2012 J. Phys.: Condens. Matter 24 284132

(http://iopscience.iop.org/0953-8984/24/28/284132)

IOP PUBLISHING JOURNAL OF PHYSICS: CONDENSED MATTER
J. Phys.: Condens. Matter **24** (2012) 284132 (8pp) doi:10.1088/0953-8984/24/28/284132

Thermophoresis of colloids by mesoscale simulations

Daniel Lüsebrink, Mingcheng Yang and Marisol Ripoll

Theoretical Soft-Matter and Biophysics, Institute of Complex Systems, Forschungszentrum Jülich, 52425 Jülich, Germany

E-mail: m.ripoll@fz-juelich.de

Received 2 December 2011, in final form 8 March 2012
Published 27 June 2012
Online at stacks.iop.org/JPhysCM/24/284132

Abstract
The motion of a colloid induced by a temperature gradient is simulated by means of multiparticle collision dynamics, a mesoscale simulation technique. Two algorithms to quantify the thermophoretic behavior are employed and contrasted. The validity of the methods is verified as a function of the temperature gradient, system size, and algorithm parameters. The variation of the solvent–colloid interaction from attractive to purely repulsive interestingly results in the change of the colloid behavior from thermophobic to thermophilic.

(Some figures may appear in colour only in the online journal)

1. Introduction

The motion of a particle due to the presence of a temperature gradient is known as thermophoresis, thermodiffusion, or the Soret effect [1]. Historically this effect has found a large number of very different applications such as isotope separation of gases [2], crude oil characterization [3], or separation of macromolecules in solution [4]. More recently, the establishment of experimental techniques that allow temperature control at small scales is originating the development of microfluidic applications [5, 6].

Thermodiffusion of colloids has been extensively investigated by means of various experimental techniques [7–10], different analytical approaches [11–15], and recently also by means of one type of atomistic simulation [16]. Most colloids in solution show a *thermophobic* behavior, that is, they tend to migrate to cold areas, although examples of *thermophilic* colloids, which tend to migrate to warm areas, can also be found [17, 18]. The particularities of the interactions between the colloid and the surrounding solvent have been shown to determine their thermophoretic behavior. Properties such as the colloidal interfacial tension, solvent polarity, colloidal charge, average temperature, or particle size, strongly influence the form of the related thermophoretic forces. Moreover, systems with varying colloidal concentration have shown that also colloid–colloid interactions can contribute significantly to the thermodiffusive properties of the solution [19, 20, 18]. So far no general theoretical explanation has been found that can predict the direction or strength of the diffusive migration of the colloids along the temperature gradient. Simulations with well-defined interactions and individually tunable parameters are therefore a promising approach to help in identifying the mechanisms and driving forces of colloidal thermodiffusion.

In this work we perform simulations with a mesoscale simulation method known as multiparticle collision dynamics (MPC) [21], which has been shown to properly include the effect of hydrodynamic interactions in colloidal and polymeric systems [22–25], and to be able of sustaining temperature inhomogeneities [26, 27]. Existing simulations of colloids in temperature gradients [28, 16] are performed with molecular dynamics (MD) of both the colloidal and the solvent particle. Coarse grained methods alternative to MPC, such as lattice Boltzmann (LB) [29, 30] or dissipative particle dynamics (DPD) [31, 32], are isothermal in their most extended implementations, although corresponding modifications to these models have been proposed in order to be able to sustain temperature inhomogeneities both for LB [33, 34] and DPD [35–37]. The rest of the paper is organized as follows. The simulation model is described in section 2 and the two methods employed to quantify the thermal diffusion factor in a dilute colloidal suspension are described in sections 3 and 4, where the validity of both methods is investigated and results with repulsive interactions between the colloid and the surrounding solvent are shown to be thermophilic. Section 5 presents simulation

results showing attractive colloid–solvent interactions are thermophobic, and a heuristic argument to understand this behavior is discussed. In section 6 we show that the finite-size effects present in these simulations enhance the value of the thermal diffusion factor, oppositely to what commonly occurs when determining transport coefficients in isothermal simulations.

2. Simulation model

In this work we perform simulations with a hybrid algorithm, employing the coarse grained solvent provided by the mesoscale method MPC [21], which is also known in the literature as stochastic rotation dynamics (SRD) [38, 25]. Colloids are considered by means of MD such that the effect of varying colloid–solvent interactions can be straightforwardly investigated. In the absence of temperature inhomogeneities the method is now well-established [25, 39, 40], and it is very successful in numerous applications of complex fluids in equilibrium [22, 24] and non-equilibrium conditions [23, 41–43].

2.1. MPC solvent

The mesoscopic MPC fluid consists of N point particles of constant mass m_i in a box of volume V. The particle state is described by its position $\mathbf{r}_i$ and velocity $\mathbf{v}_i$ $(i = 1, \ldots, N)$, which can vary continuously in phase space. The dynamics takes place in two alternating steps. In the *streaming step* particles evolve ballistically during a certain time h, the *collision time*, $\mathbf{r}_i(t+h) = \mathbf{r}_i(t)+h\mathbf{v}_i(t)$. In the *collision step* the simulation box is divided into cubic collision boxes in which the particles are sorted. All particles j within the collision box of particle i at a certain time step, interact with each other through the center-of-mass velocity of the collision box, $\mathbf{v}_{\mathrm{cm},i}(t) = \sum_j^i m_j\mathbf{v}_j(t)/\sum_j^i m_j$. The actual collision considers a rotation of the relative velocity to the center-of-mass velocity by an angle α, around a random orientation,

$$\mathbf{v}_i(t+h) = \mathbf{v}_{\mathrm{cm},i}(t) + \mathcal{R}(\alpha)[\mathbf{v}_i(t) - \mathbf{v}_{\mathrm{cm},i}(t)], \qquad (1)$$

with $\mathcal{R}(\alpha)$ the stochastic rotation matrix. This simple collision rule strictly imposes conservation of mass, linear momentum, and kinetic energy at the collision box level. This ensures the presence of hydrodynamic interactions, together with the sustainability of temperature gradients and thermal fluctuations. In order to preserve Galilean invariance and enhance collisional transport, a *random shift* of the collision box grid is additionally considered [38]. The reference units are chosen to be the particle mass m, the collision box size a and a reference temperature T, which are typically set to one. This corresponds to a length measure as $\hat{x} = x/a$ and time measure as $\hat{t} = t\sqrt{k_\mathrm{B}T/ma^2}$, with k_B the Boltzmann constant. Kinetic theory calculations [44–46] have very successfully related the MPC parameters to the corresponding transport properties of the MPC fluid. These parameters are the collision time h, the rotation angle α, and the particle density $\rho = N/V$. The non-potential interactions between the MPC particles describe a fluid with the ideal gas equation of state for all parameters. Nevertheless, the range of parameters with large values of α and small values of h has been shown to display a liquid-like behavior characterized by large values of the Schmidt number $Sc = \nu/D$, with ν the kinematic viscosity and D the diffusion coefficient [22, 47]. In this work we use a unique set of parameters to describe the MPC solvent, $h = 0.1, \alpha = 120°$, and $\rho = 10$, which in three dimensions corresponds to $Sc = 13$.

2.2. Temperature gradient establishment

We consider a three dimensional system with periodic boundary conditions, with a temperature gradient imposed in one of them. This is obtained by defining a *cold* layer with temperature T_c at one extreme of the box, and a *hot* layer with temperature $T_\mathrm{h} > T_\mathrm{c}$ at the center of the box. In this way the simulation box is divided in two half boxes with increasing temperatures towards the center. The system dimensions are identified as $L_\perp$ in the two directions perpendicular to the temperature gradient and $2L_z$ in the gradient direction. The temperature at the cold and hot layers is not directly imposed but is a consequence of an energy flux which is imposed by the so-called velocity exchange algorithm. The method was originally introduced in the framework of MD simulations [48, 49], and consists in identifying the hottest particle of the cold layer and the coldest particle of the warm layer, then interchanging their velocities, as a type of *Maxwell's demon*. More details on this and other possible implementations of the temperature gradient within the MPC fluid can be found in [26, 27]. After a certain time, the system in contact with the thermal baths reaches a steady linear temperature profile

$$T(z) = T_\mathrm{c} + \nabla T z, \qquad (2)$$

where $\nabla T = (T_\mathrm{h}-T_\mathrm{c})/L_z$ is the resulting temperature gradient in the z-direction, and L_z is the distance between the two baths. The equation of state of an MPC fluid is that of an ideal gas, which determines the density distribution as $\rho(z) = p/k_\mathrm{B}T(z)$, with p the system pressure. In the limit of small temperature differences, the density profile can be approximated by a linear function decreasing in the direction of increasing temperature.

2.3. Colloid implementation

In this work, the interaction between the colloid and the surrounding MPC solvent is performed by means of MD. This means that the solvent particles in the colloid interaction range update their positions with the MD integration algorithm, velocity-Verlet in our case, instead of with the MPC streaming step, then taking part only in the collision step [50]. The MD integration time step Δt should be small enough to integrate the corresponding potential, although there is no further dependence on it. Typical values are $h/\Delta t = 50, 100, 200$, depending on the potential. The employed interaction potential is varied to explore the effect of attractive

and repulsive interactions, and in both cases we employ a Lennard-Jones (LJ) type of potential,

$$U(r) = 4\epsilon\left[\left(\frac{\sigma}{r}\right)^{2n} - \left(\frac{\sigma}{r}\right)^{n}\right] + C, \qquad r < r_c, \quad (3)$$

with r the distance between the solvent particle and the colloid center. The potential intensity is here always chosen as $\epsilon = k_B\bar{T} = 1$, with $\bar{T}$ the average temperature, and the colloidal radius is varied from $\sigma = 1$ to 4. The repulsive potential is characterized with the standard values $C = \epsilon, n = 6$, and $r_c = 2^{1/6}\sigma$. The attractive potential is defined by $C = 0$, and we consider $n = 48$. The value of the exponent is here selected especially high in order to limit the range of attraction and therefore the number of interacting solvent particles. The cut-off radius is matched at the point where the potential is as small as the standard LJ $n = 6$ potential. In this way, we define $\tilde{U} = U^{n=6}(r = 2.5\sigma)$, such that $r_c = [2/(1 - \sqrt{1 + \tilde{U}})]^{1/6}\sigma$. The mass density of the colloid is fixed to be neutrally buoyant, in other words the same as the mass density of the solvent. The colloid mass then ranges from $m_c = 42$ for $\sigma = 1$ up to $m_c = 2680$ for $\sigma = 4$. Furthermore, it should be noted that with the actual boundary conditions the main box is divided into two halves with temperature gradients in opposite directions. In order to keep this symmetry, each colloid needs to be accompanied by a *twin* neighbor in the other half simulation box, besides all the corresponding periodic images.

3. Single particle thermodiffusion algorithm

The basic phenomenological equation that describes the thermodiffusion phenomena [51] of a two-component mixture characterizes the particle flux J of component one in the direction of a temperature gradient ∇T as

$$J = -\tilde{n}D_m\nabla x - \tilde{n}D_T x(1 - x)\nabla T, \quad (4)$$

where $\tilde{n} = n + n'$ is the averaged total number density, with n and n' the densities of the two components, $x = n/\tilde{n}$ the molar fraction of component one, D_m the mutual diffusion coefficient, and D_T the thermal diffusion coefficient. The so-called Soret coefficient is defined as the ratio of the two diffusion coefficients

$$S_T \equiv \frac{D_T}{D_m}, \quad (5)$$

and indicates how strongly the two components separate. In the stationary state, the particle flux vanishes, and the Soret coefficient can be obtained from the molar fraction and temperature distribution

$$S_T = -\frac{1}{x(1 - x)}\frac{\nabla x}{\nabla T}. \quad (6)$$

Note that, by convention, a positive S_T indicates that for component one the relative accumulation is higher on the cold side, while a negative S_T will display a reciprocal behavior. Equation (6) constitutes the standard method to quantify the thermodiffusion phenomena in concentrated mixtures. Nevertheless, in the case of dilute solutions the determination of the density profiles that define the molar fraction gradient are not feasible to compute, such that specific methods need to be developed.

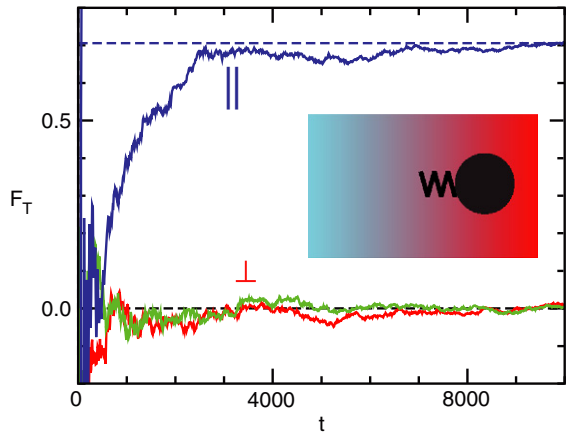

Figure 1. Thermophoretic force as a time average versus time for a colloid attached to a spring with repulsive interactions with the solvent. Colloid diameter $d = 6$, temperature gradient $\nabla T = 0.007$, and system size $L_\perp = L_z = 42$.

In a recent study Galliéro and Volz [16] proposed a method called the single particle thermodiffusion algorithm (SPTA) to measure the thermal diffusion factor. The idea is that by attaching the particle to a harmonic spring, there is no average drift velocity. The thermophoretic force $\mathbf{F}_T$ then balances the harmonic force $\mathbf{F}_H$, which can be determined as $\mathbf{F}_T = -\mathbf{F}_H = k\Delta\mathbf{r}$, where k is the harmonic constant and $\Delta\mathbf{r}$ the average deviation of the colloid from its neutral position. One example of the averaged $\mathbf{F}_T$ is displayed in figure 1 for a colloid with repulsive interactions with the surrounding solvent. The instantaneous forces fluctuate strongly, such that here we display the time integral, with values averaged over 24 simulations. In the two perpendicular directions to the temperature gradient the force vanishes, while in the parallel direction to the gradient the averaged force has a clear positive value whose long-time behavior we account for as the computed thermophoretic force F_T. The positive value of the force indicates that the colloid goes on average towards the hot bath, i.e. it is *thermophilic*.

The influence of the strength of the spring on the measured force is analyzed by performing simulations with different spring constants k. In figure 2, computed values F_T are shown as a function of the inverse k. Within the error of the measurements, it can be observed that there is no influence of the spring constant. Moreover, no significant difference is observed in the case that the colloid is completely fixed ($k \to \infty$). The force in this case is calculated as the average force exerted on the colloid by all surrounding solvent particles.

The relation of this force to the thermal diffusion factor can be obtained by taking several standard assumptions. One is that, in the absence of the spring, the thermophoretic force F_T would balance with the friction force $F_\zeta = -\zeta v_T$. Then the friction coefficient ζ can be understood to be related to the self-diffusion coefficient by the Einstein relation, $D_s = k_B T\zeta$. Lastly, the thermophoretic velocity v_T is considered to be proportional to the thermodiffusion coefficient,

$$v_T = -D_T\nabla T. \quad (7)$$

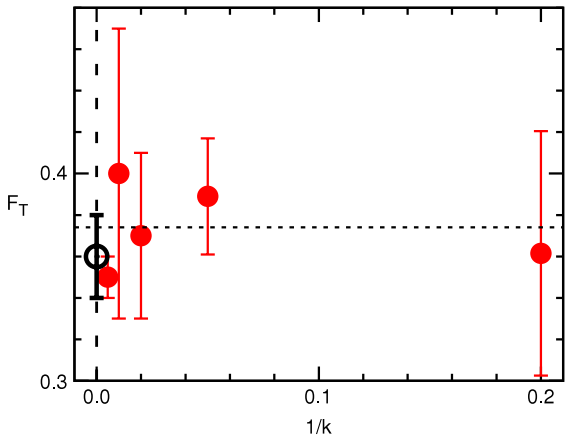

Figure 2. Dependence of the thermophoretic force on the spring strength. Colloid with solvent repulsive interactions, diameter $d = 4$, temperature gradient $\nabla T = 0.01$ and system size $L_\perp = 10, L_z = 30$. Solid symbols are simulation results with a spring of finite spring constant, the empty symbol corresponds to a fixed colloid, and the dashed line is the averaged value.

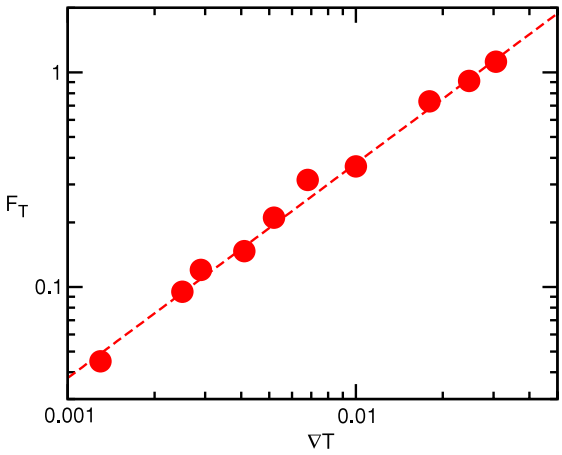

Figure 3. Dependence of the thermophoretic force on the temperature gradient. Dashed line corresponds to a linear fit. Colloid with solvent repulsive interactions, diameter $d = 4$, and system size $L_\perp = 10, L_z = 30$.

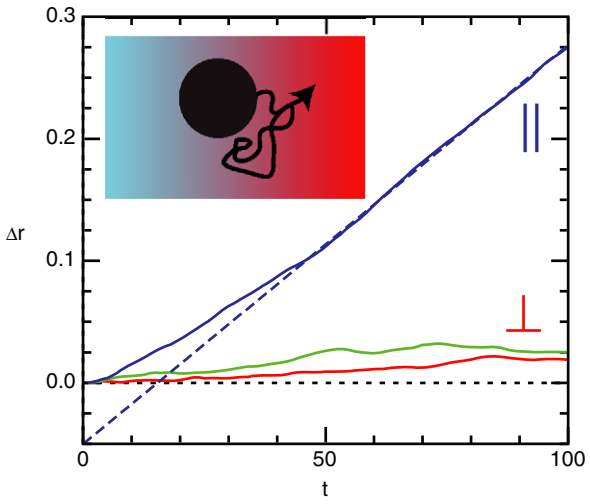

Figure 4. Average mean displacement of a free colloid as a function of time. Continuous lines are the average over 2016 simulations. Dashed line corresponds to a linear fit of the simulation data for $t \geq 50$. Simulation parameters are similar to those in figure 1.

This expression will be discussed later. These relations, together with the definitions of the Soret coefficient in equation (5) and the dimensionless thermal diffusion factor $\alpha_T = \bar{T} S_T$, lead to

$$F_T = -\alpha_T \nabla k_B T. \tag{8}$$

The same relation can also be exactly obtained through an alternative route based on the van Kampen mass flux equation for inhomogeneous systems [52]. The only necessary additional consideration is that the thermophoretic force exerted on an MPC solvent particle is exactly vanishing due to its ideal gas nature [53].

In order to test the validity of the method, we check the linear relation of the force and the temperature gradient. The results are shown in figure 3 and prove that the system is within the linear response regime in all employed temperature gradients, such that α_T in equation (8) is well defined. Note, however, that much larger temperature differences between the thermal baths than those shown here might be too large and also provide strongly non-linear density profiles. Decreasing the value of the temperature gradient increases the relative importance of the thermal fluctuations such that more averaging is necessary to obtain a reasonable value of the thermophoretic force.

4. Drift velocity measurements

The evaluation of the thermal diffusion factor at dilute concentrations with more than one colloid can require a method in which the colloids are freely moving, which can also help in understanding the eventual effect of the previously considered spring. When the colloid position is not averagely fixed, the thermophoretic force translates with a drift velocity, which balances with a friction force, such that a vanishing total force is exerted on the colloid. In this case, the measurement of the average drift velocity of the particle v_d can be approximately related to thermodiffusion coefficient by equation (7).

We perform simulations by initially releasing one colloid in each of the two half boxes, equidistant from the cold and hot thermal baths. The velocity is computed by quantifying the average particle displacement as a function of time. The total computed time should then be large enough for the colloid to have approached the steady state, but short enough to ensure that it has not reached any of the thermal baths. This time is therefore much shorter than for the simulations employing the SPTA, such that the typical number of required averaging runs is much larger. Figure 4 shows one example of the averaged mean displacement as a function of time for a colloid with repulsive interactions between colloid and solvent and essentially the same parameters as those shown for figure 1. The mean displacement vanishes in the two directions perpendicular to the temperature gradient. In

Table 1. Comparison of results obtained with the SPTA and thermophoretic velocity measurements, together with the employed D_s values.

d	SPTA $\rightarrow \alpha_T$	$v_T \rightarrow \alpha_T$	$10^3 D_s$
2	−5.7	−5.0	14.8
4	−29	−24	6.7
6	−104	−120	3.9
8	−243	−258	2.8

the ∇T-direction, the mean displacement increases, and this increase is linear for long enough times. The slope of the linear growth allows us to clearly identify v_d.

A series of simulations with both the SPTA and the thermophoretic velocity method are performed to check the consistency of these algorithms. The value of the thermal diffusion factor is obtained directly from the thermophoretic force with equation (8). Meanwhile, the measurements of the thermophoretic velocity are related to α_T with equations (5) and (7) as

$$\alpha_T \simeq -\frac{\bar{T}}{D_s}\frac{v_T}{\nabla T}. \tag{9}$$

In the considered case of a very dilute colloidal suspension, the mutual diffusion coincides with the colloid self-diffusion coefficient, which needs to be further quantified. The employed values of D_s are obtained by determining the averaged mean squared displacement in additional equilibrium simulations. A summary of the quantified values is presented in table 1. The results show a good agreement between both methods within the precision of the simulations. This agreement verifies the viability of both algorithms within the validity restrictions of the performed approximations, as above discussed.

Galliéro and Volz [16] perform MD simulations with colloidal suspensions at varying concentrations and evaluate the Soret coefficient S_T with the standard method in equation (6). The extrapolation of their data to the infinitely dilute case agrees well with the value obtained with the SPTA, apart from a small underestimation whose origin is discussed in [53]. Although we have not performed a similar study with either of the two algorithms presented here, it is reasonable to accept the results in [16] as a validation for the method.

The thermal diffusion factor α_T calculation presented in this section relies on the definition of the thermophoretic velocity in equation (7). This equation has been shown from two different approaches [54, 55] to be just an approximation of the more precise expression,

$$v_d = -D_T\nabla T - D_s\beta_T\nabla T + \nabla D_s, \tag{10}$$

where β_T is the thermal expansion coefficient. The two additional terms can be neglected in the cases where $|D_T| \gg |\mathrm{d}D_s/\mathrm{d}T - D_s\beta|$, which is indeed the case in most complex fluids [5, 56, 57]. We quantify here the validity of this approximation through the related equation of the thermal diffusion factor obtained with equation (5),

$$\alpha_T = -\frac{\bar{T}}{D_s}\frac{v_d}{\nabla T} - \bar{T}\beta_T + \frac{\bar{T}}{D_s}\frac{\partial D_s}{\partial T}. \tag{11}$$

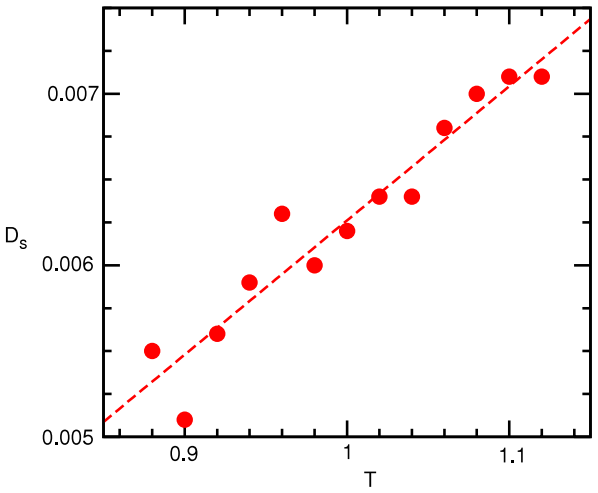

Figure 5. Colloid self-diffusion coefficient D_s from equilibrium simulations at various temperatures. Colloid diameter $d = 4$.

The first term corresponds to the quantity already evaluated in the third column of table 1. The second term is exactly equal to one, since the thermal expansion coefficient for the MPC solvent is known to be $\beta_T = 1/\bar{T}$. The last term can obtained from equilibrium simulations of D_s at different temperatures, as shown in figure 5. These results quantify that $\partial D_s/\partial T = 0.0059$ for a colloid with diameter $d = 4$, and $D_s = 0.0067$ for $T = 1$. This means that the contribution of the two last terms can be calculated to be approximately 0.5% of the first one, which is in fact smaller than the error of our simulations.

A different aspect which is important to take into account is that the thermophoretic force on the colloids translates into the presence of a thermophoretic flow field opposite to it [58–60]. For the case of a fixed colloid, this flow decays as r^{-1}, the inverse distance, similar to the standard propagation of hydrodynamic interactions. Meanwhile, in the case of the moving colloid, this flow will decay as r^{-3}; therefore much faster.

In order to give a comparative statement for the choice of one of these methods in future applications, we should point out that from the computational cost point of view both methods are similar in principle. The differences arise from two aspects. One is that the data is easier to analyze in the SPTA since the force on the colloid is constant after equilibration, whereas the drift is only constant after the Brownian time scale, and before the colloid feels the effect of the boundaries, which translates as an additional effort. Another aspect is that the SPTA directly evaluates the thermophoretic force F_T, and thus the thermal diffusion factor α_T, while the evaluation of the drift velocity results in a good approximation of the thermodiffusion coefficient D_T. This may result in the convenience of one of the methods, since the additional determination of the self-diffusion coefficient could be avoided in some cases.

5. Attractive colloid–solvent interactions

In the previous sections we have presented results with repulsive interactions between the colloid and the surrounding

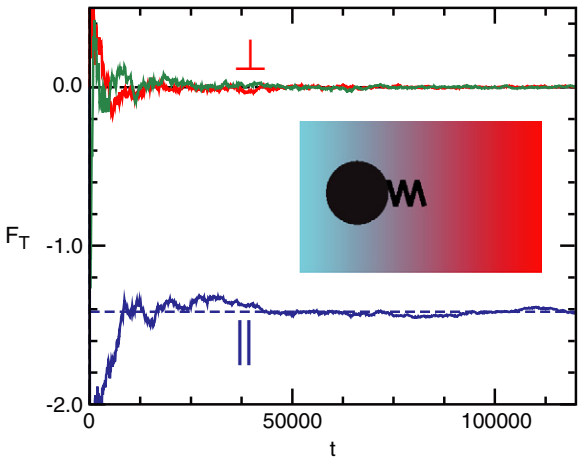

Figure 6. Thermophoretic force as a time average versus time for a colloid attached to a spring with attractive interactions with the solvent. Colloid diameter $d = 6$, and system size $L_\perp = L_z = 42$.

Table 2. Summary of result obtained with the SPTA with attractive colloid–solvent interactions.

d	SPTA $\rightarrow \alpha_T$
2	7.0
4	65
6	197
8	440

solvent, which have been shown to translate into a *thermophilic* behavior. Here we discuss the effect of attractive interactions, which have been implemented by employing a LJ type potential as stated in equation (3). The preliminary obtained results display negative thermophoretic forces, as can be seen in figure 6 and in table 2. This indicates that the colloid goes on average to the cold areas, in other words it becomes *thermophobic*. Previous simulations [16] with a purely MD model with attractive interactions have reported only such thermophobic behavior.

Experimentally, a similar influence of the attraction interaction between solute and solvent on the thermodiffusive properties has been observed in polymeric systems with different solvents [61–64]. Although polymers are mostly thermophobic [65, 57], in cases where the affinity between solute and solvent is higher the Soret coefficients are found to be larger, while in cases where the affinity is reduced, for example by diminishing the relevance of the hydrogen bonds in water-based solutions, the Soret coefficient can become eventually negative [61].

An intuitive picture to understand the behavior obtained in our simulation results can be drawn as follows. In general situations, and very especially in MPC, the solvent density in the warm region is smaller than that in the cold region, as illustrated in figure 7. The larger number of particles on the low-temperature side of the particle may then produce stronger interactions than on the warm side. Therefore, the repulsive colloid–solvent interactions push the colloid towards high temperatures, while attractive colloid–solvent interactions pull the colloid to low temperatures. This simple

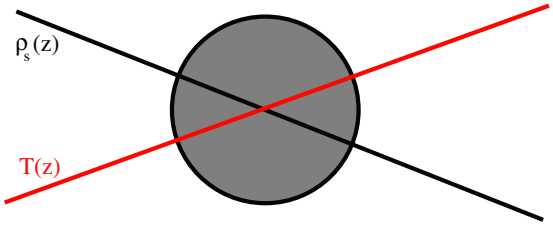

Figure 7. Schematic of a colloid with its surrounding MPC solvent density in the presence of a temperature gradient.

intuitive picture is, however, not generally valid since it ignores the strength of the collisions at different temperatures. A more in-depth study will be presented elsewhere.

The thermal diffusion factor α_T in tables 1 and 2 clearly increases with the particle size. Although it is not the main goal of this work to investigate this dependence, from our data a cubic dependence can be inferred for both attractive and repulsive interactions. This is in contrast to experimental and analytical results [8–10] in which this dependence is debated to be between quadratic and linear. Preliminary results [26] indicate that the cubic dependence is due to the nature of the Lennard-Jones interaction employed in this work, such that a different colloid–solvent interaction will noticeably vary in its dependence, as we will discuss in detail in a forthcoming publication.

6. Finite system size effects

The finiteness of the simulation box has two principal effects on the transport properties of the equilibrium systems [66–68]. In an infinite system, perturbations of arbitrary wavelengths can propagate, while, in a finite system, the maximum wavelengths are determined by the system size $k_{max} = 2\pi/L$. This truncation of the propagation spectra results in a faster decay of the correlation functions and consequently in a slow down of the transport properties. Faster decay of the correlation functions dependent on the system size has been observed in various systems [69, 47, 70–72]. Diffusion of polymers constitute a reference example of this effect [73, 24], where a box-size-dependent hydrodynamic radius emerges to describe the effective polymer center-of-mass diffusion coefficient. When periodic boundary conditions are employed, each particle in the system interacts with an infinite number of periodic images. This effect translates in an increase of the auto-correlation functions, then having an opposite effect to the spectra truncation. Nevertheless, the contribution of the periodic images appears at later times, having a negligible effect in comparison with the spectra truncation. The general trend is then that the related transport coefficients increase with the box size. To avoid the effect of the periodic images, systems can be considered to be placed between walls, although in that case the effects due to confinement can become much more relevant.

In order to investigate finite-size effects in our simulations with temperature gradients, we compute the thermal diffusion factor α_T for a fixed particle diameter ($d =$

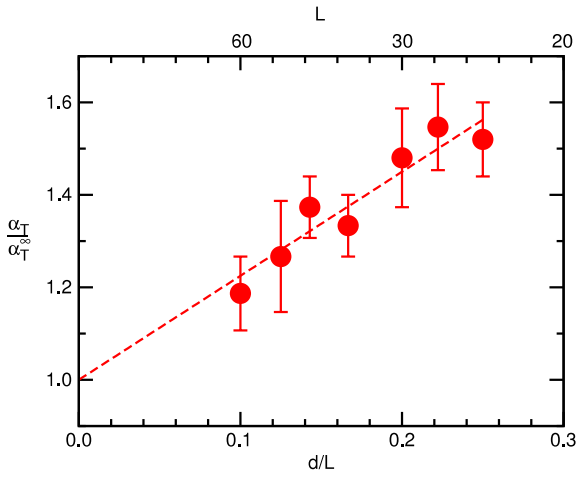

Figure 8. Normalized thermal diffusion coefficient versus the ratio of particle diameter over system size. The simulations have been performed with the SPTA with colloid diameter $d = 6$, and repulsive colloid–solvent interaction. Symbols correspond to simulation computed values, and the dashed line is the linear extrapolation of equation (12), with $\alpha_T^\infty = -75$ and $\lambda = 2.2$.

6), varying the simulation box size with the SPTA method. The employed box is a double cube with $L_\perp = L_z$. Figure 8 shows a normalized thermal diffusion factor as a function of the inverse system size in units of the colloid diameter d/L_z, which can be approximated by the following linear behavior

$$\alpha_T = \alpha_T^\infty \left(1 + \lambda \frac{d}{L_z}\right). \tag{12}$$

Here α_T^∞ is the value of the thermal diffusion factor extrapolated to an infinitely large system and λ is the scaling factor. The value of α_T^∞ defines the thermodiffusion of the system such that it then depends on system properties such as the colloid size, strength and type of interaction, or average temperature. The scaling factor does not necessary depend on the same properties, since it accounts for the finite-size effect, although more detailed simulations are still required to verify this statement.

Apart from the strong finite-size dependence, the most remarkable characteristic of the results shown in figure 8 is that the absolute value of the thermal diffusion factor decreases with the box size. This is in contrast to other quantities, such as the center-of-mass diffusion of a polymer in an equilibrium state, which increases with the box size [73, 24]. Besides the effects discussed above, one needs to consider that with the actual implementation of the temperature gradient it implies that each colloid is accompanied by a *twin* neighbor in the other half simulation box with thermophoretic forces opposite to each other. More importantly, each of these colloids is accompanied by the corresponding thermophoretic fluid flow, which has opposite direction to the thermophoretic force. It is then reasonable to assume that the presence of the twin colloids and their generated flow fields enhance the value of the thermal diffusion factor, an effect that decreases with increasing system size. This would explain an overall decrease of the thermal diffusion factor with the box size, in agreement with the results shown in figure 8. The values of α_T presented in tables 1 and 2 for different colloidal diameters are performed keeping the ratio d/L_z constant, in particular the box size is varied to be $L_z = 6d$.

In the case of the moving particle, the thermophoretic flow decays much faster than for the SPTA and then the finite-size effects in determining D_T are expected to be much smaller. For the results presented in table 1 it should, however, be considered that the determination of D_s is also required. The self-diffusion coefficient is also known to be importantly affected by finite-size effects, which linearly increase its value with system size [25]. Since α_T depends on the inverse of D_s, a similar decrease with system size as for the SPTA is expected. This argument is supported also by the nice agreement between both methods in table 1, where the finite-size effects should be comparable since the employed system sizes are the same in both cases.

7. Conclusions

Simulations of colloidal solutions in the dilute regime are performed with a hybrid mesoscopic model, as an alternative to the existing MD simulations. The thermal diffusion factor is quantified using two different algorithms. One consists in attaching the colloid to a harmonic spring and then quantifying the average spring deformation, and the other consists in computing the average drift velocity of a free colloid. The consistency shown by each of the algorithms, together with the satisfactory agreement between them, confirms these two methods as a reliable way of obtaining the thermal diffusion properties in the dilute regime. These methods can, and have already been, experimentally employed, using laser tweezers to determine the thermophoretic force [74] or by following the colloids trajectories with an appropriate microscopy [5]. We investigate the finite-size effects present in our simulations, which are shown to enhance the value of the thermal diffusion factor, in contrast to the common behavior in isothermal simulations. We argue that the main difference stems from the particular periodic boundary conditions in the presence of a temperature gradient, where the simulation box is divided into two halves with temperature gradients of opposite slopes, each colloid is accompanied by a twin neighbor, both undergoing thermophoretic forces and fluid flows in opposite directions. Simulation results of colloids with a purely repulsive interaction with the surrounding solvent are shown to be thermophilic, while colloids with attractive colloid–solvent interactions are shown to be thermophobic. This behavior can be compared with experimental observations and are explained from an heuristic argument. Furthermore, the different thermal affinities shown by our model can be exploited to build thermophoretic microswimmers with pulling or pushing behavior, as shown in [75, 76], which will contribute in the development of synthetic nanomachines.

Acknowledgments

The authors are grateful for valuable discussions with Simone Wiegand, Ulf D Schiller, and Gerhard Gompper.

References

[1] Wiegand S 2004 *J. Phys.: Condens. Matter* **16** R357–79
[2] Clusius K and Dickel G 1938 *Naturwissenschaften* **26** 546–6
[3] Ghorayeb K, Firoozabadi A and Anraku T 2003 *SPE J.* **8** 114–23
[4] Giddings J 1993 *Science* **260** 1456–65
[5] Duhr S and Braun D 2006 *Proc. Natl Acad. Sci.* **103** 19678–82
[6] Jiang H R, Wada H, Yoshinaga N and Sano M 2009 *Phys. Rev. Lett.* **102** 208301
[7] Piazza R and Guarino A 2002 *Phys. Rev. Lett.* **88** 208302
[8] Duhr S and Braun D 2006 *Phys. Rev. Lett.* **96** 168301
[9] Putnam S A, Cahill D G and Wong G C L 2007 *Langmuir* **23** 9228
[10] Braibanti M, Vigolo D and Piazza R 2008 *Phys. Rev. Lett.* **100** 108303
[11] Bringuier E and Bourdon A 2003 *Phys. Rev.* E **67** 011404
[12] Bringuier E and Bourdon A 2007 *J. Non-Equilib. Thermodyn.* **32** 221–9
[13] Dhont J K G, Wiegand S, Duhr S and Braun D 2007 *Langmuir* **23** 1674
[14] Dhont J K G and Briels W J 2008 *Eur. Phys. J.* E **25** 61
[15] Würger A 2009 *Langmuir* **25** 6696
[16] Galliéro G and Volz S 2008 *J. Chem. Phys.* **128** 064505
[17] Piazza R and Parola A 2008 *J. Phys.: Condens. Matter* **20** 153102
[18] Ning H, Buitenhuis J, Dhont J K G and Wiegand S 2006 *J. Chem. Phys.* **125** 204911
[19] Dhont J K G 2004 *J. Chem. Phys.* **120** 1632–41
[20] Dhont J K G 2004 *J. Chem. Phys.* **120** 1642–53
[21] Malevanets A and Kapral R 1999 *J. Chem. Phys.* **110** 8605–13
[22] Ripoll M, Mussawisade K, Winkler R G and Gompper G 2004 *Europhys. Lett.* **68** 106–12
[23] Padding J T and Louis A A 2004 *Phys. Rev. Lett.* **93** 220601
[24] Mussawisade K, Ripoll M, Winkler R G and Gompper G 2005 *J. Chem. Phys.* **123** 144905
[25] Padding J T and Louis A A 2006 *Phys. Rev.* E **74** 031402
[26] Lüsebrink D 2011 Colloidal suspensions in temperature gradients with mesoscopic simulations *PhD Thesis* Cologne University, Germany
[27] Lüsebrink D and Ripoll M 2012 *J. Chem. Phys.* **136** 084106
[28] Vladkov M and Barrat J L 2006 *Nano Lett.* **6** 1224–8
[29] McNamara G R and Zanetti G 1988 *Phys. Rev. Lett.* **61** 2332
[30] Succi S 2001 *The Lattice Boltzmann Equation: For Fluid Dynamics and Beyond* (Oxford: Clarendon)
[31] Hoogerbrugge P J and Koelman J M V A 1992 *Europhys. Lett.* **19** 155–60
[32] Español P and Warren P 1995 *Europhys. Lett.* **30** 191
[33] Alexander F J, Chen S and Sterling J D 1993 *Phys. Rev.* E **47** 2249(R)
[34] Lallemand P and Luo L S 2003 *Phys. Rev.* E **68** 036706
[35] Español P 1997 *Europhys. Lett.* **40** 631
[36] Bonet-Avalós J and Mackie A D 1997 *Europhys. Lett.* **40** 141
[37] Ripoll M and Ernst M H 2005 *Phys. Rev.* E **71** 041104
[38] Ihle T and Kroll D M 2001 *Phys. Rev.* E **63** 020201(R)
[39] Kapral R 2008 *Adv. Chem. Phys.* **140** 89–146
[40] Gompper G, Ihle T, Kroll D M and Winkler R G 2009 *Adv. Polym. Sci.* **221** 1–87
[41] Noguchi H and Gompper G 2005 *Proc. Natl Acad. Sci.* **102** 14159–64
[42] Ripoll M, Winkler R G and Gompper G 2006 *Phys. Rev. Lett.* **96** 188302
[43] Ripoll M, Holmqvist P, Winkler R G, Gompper G, Dhont J K G and Lettinga M P 2008 *Phys. Rev. Lett.* **101** 168302
[44] Tüzel E, Strauss M, Ihle T and Kroll D M 2003 *Phys. Rev.* E **68** 036701
[45] Kikuchi N, Pooley C M, Ryder J F and Yeomans J M 2003 *J. Chem. Phys.* **119** 6388–95
[46] Tüzel E, Ihle T and Kroll D M 2006 *Phys. Rev.* E **74** 056702
[47] Ripoll M, Mussawisade K, Winkler R G and Gompper G 2005 *Phys. Rev.* E **72** 016701
[48] Hafskjold B, Ikeshoji T and Ratkje S K 1993 *Mol. Phys.* **80** 1389–412
[49] Müller-Plathe F 1997 *J. Chem. Phys.* **106** 6082–5
[50] Lee S H and Kapral R 2006 *J. Chem. Phys.* **124** 214901
[51] de Groot S R and Mazur P 1984 *Nonequilibrium Thermodynamics* (New York: Dover)
[52] van Kampen N 1988 *J. Phys. Chem. Solids* **49** 673
[53] Yang M and Ripoll M 2012 *J. Phys.: Condens. Matter* **24** 195101
[54] Bringuier E and Bourdon A 2007 *Physica* A **385** 9–24
[55] Yang M and Ripoll M 2012 *J. Chem. Phys.* at press
[56] Würger A 2010 *Rep. Prog. Phys.* **73** 126601
[57] Stadelmaier D and Köhler W 2008 *Macromolecules* **41** 6205–9
[58] Weinert F M and Braun D 2008 *Phys. Rev. Lett.* **101** 168301
[59] Di Leonardo R, Ianni F and Ruocco G 2009 *Langmuir* **25** 4247
[60] Yang M and Ripoll M 2012 in preparation
[61] de Gans B J, Kita R, Wiegand S and Luettmer-Strathmann J 2003 *Phys. Rev. Lett.* **91** 245501
[62] de Gans B J, Kita R, Müller B and Wiegand S 2003 *J. Chem. Phys.* **118** 8073–81
[63] Sugaya R, Wolf B A and Kita R 2006 *Biomacromolecules* **7** 435–40
[64] Kita R, Polyakov P and Wiegand S 2007 *Macromolecules* **40** 1638–42
[65] Rauch J and Köhler W 2005 *Macromolecules* **38** 3571–3
[66] Ladd A J C 1990 *J. Chem. Phys.* **93** 3484
[67] Dünweg B and Kremer K 1991 *Phys. Rev. Lett.* **66** 2996
[68] Pierleoni C and Ryckaert J 1992 *J. Chem. Phys.* **96** 8539
[69] Ripoll M and Ernst M H 2005 *Phys. Rev.* E **72** 011101
[70] Sané J, Padding J T and Louis A A 2009 *Phys. Rev.* E **79** 051402
[71] Heyes D M, Cass M J, Powles J G and Evans W A B 2007 *J. Phys. Chem.* B **111** 1455
[72] Isobe M 2008 *Phys. Rev.* E **77** 021201
[73] Dünweg B and Kremer K 1993 *J. Chem. Phys.* **99** 6983
[74] Jiang H R 2011 private communication
[75] Jiang H R, Yoshinaga N and Sano M 2010 *Phys. Rev. Lett.* **105** 268302
[76] Yang M and Ripoll M 2011 *Phys. Rev.* E **84** 061401